Evaluating Ionospheric Effects on SBAS in the Low Magnetic Latitude Region

Takeyasu Sakai, Keisuke Matsunaga, and Kazuaki Hoshinoo, *Electronic Navigation Research Institute, Japan*
Todd Walter, *Stanford University, USA*

BIOGRAPHY

Takeyasu Sakai is a Senior Researcher of Electronic Navigation Research Institute, Japan. He received his Dr. Eng. in 2000 from Waseda University and is currently analyzing and developing ionospheric algorithms for Japanese MSAS program.

Keisuke Matsunaga is a Researcher of Electronic Navigation Research Institute. He received his M. Sc. in 1996 from Kyoto University and worked for the development of LSI at Mitsubishi Electric Corporation from 1996 to 1999. He joined ENRI in 1999, and is currently studying ionospheric effects on MSAS.

Kazuaki Hoshinoo is a Principal Researcher of Electronic Navigation Research Institute. He is the director of MSAS research program in ENRI and is a member of the MSAS Technical Review Board of JCAB. He chairs Ionosphere Working Group of the Board.

Todd Walter is a Senior Research Engineer in the Department of Aeronautics and Astronautics at Stanford University. Dr. Walter received his PhD. in 1993 from Stanford and is currently developing WAAS integrity algorithms and analyzing the availability of the WAAS signal.

ABSTRACT

The signal propagation delay caused by ionosphere is now recognized as a major error source for satellite navigation systems. Because ionosphere is generated by solar radiation and affected by the geomagnetic field, the associated signal delay is very large and has significant variance in the low magnetic latitude region. The ionospheric delay problem is currently the major concern for MSAS program (Japanese version of SBAS/WAAS) which includes the near equatorial region in its service area and therefore might experience significant performance degradation.

The current SBAS ionospheric correction procedure is based on the algorithm called as ‘planar fit’. It estimates the propagation delays at IGPs located at every five by five degrees in geographic latitude and longitude, and then broadcasts them to users within the coverage. The first order estimator, relates to ‘plane’, is used in the algorithm. This procedure is designed based on the observations and experiences over US CONUS, but we do not know how well this works in the low magnetic latitude region.

At first the authors have analyzed the actual ionospheric effects over Japan during quiet and storm conditions. According to this analysis, although the absolute signal delay and its variance are relatively large, the planar fit could describe the spatial distribution of vertical ionospheric delays very well, and resulted in variance of residuals, σ_{decorr}, of around 35-40 cm, which agrees with the value in CONUS.

Then we have evaluated the performance of the current SBAS ionospheric correction procedure over Japan. The first order (planar fit) correction does, fortunately, work well although the absolute delay is large. We also tried the second order correction but it seemed not practical.

The authors also have demonstrated the performance of the storm detector currently employed for MSAS. Even for nominal condition, most IGPs will be determined as storm conditions around Japan by the current detector. This fact implies that the detector might need to be modified slightly for improving availability of MSAS. Three candidate algorithms for alternative storm detector have been tested, and all responded with low false alarm rate relative to the current algorithm.

INTRODUCTION

The ionosphere is a plasma layer of the upper atmosphere distributed approximately 50-1,000 km above the ground. Ranging signals transmitted from GPS satellites propagate slightly slower during passage through the ionosphere, so a few to 100 meters propagation delay would be added to measured pseudorange for GPS receivers.

Ionospheric delay is now recognized as a major error source for satellite navigation systems. ICAO SBAS (satellite-based augmentation system), defined by SARPs (international standards and recommended practices) [1] documents, has a capability to make a correction to ionospheric delay effects. It would broadcast users the vertical ionospheric delay estimates in meters at the grid points (IGP; ionospheric grid point) defined at every five by five degrees in geographic latitude and longitude.

The SBAS ionospheric correction procedure was actually defined based on the observation and knowledge on the ionospheric activities over the US CONUS. In fact the ionosphere has the significant activities in the equatorial regions while CONUS located in the relatively high magnetic latitude region. The equatorial anomalies affect on the large-scale structure of electron density of ionosphere which might be difficult to be corrected by SBAS ionospheric correction messages [2]. Plasma bubble effects (also known as depletion), usually occur also in the low latitude region, might cause significant scintillation which disrupts GPS signals [3][4]. ICAO SBAS IWG (Interoperability Working Group) meeting has pointed out this problem and now has organized specialized SBAS Iono-meetings frequently.

SBAS is the international standard system for global and seamless satellite-based navigation, so it would be used even in the equatorial or low latitude regions. SBAS providers need to investigate ionospheric effects around the magnetic equator and the low magnetic latitude regions in terms of SBAS ionospheric error correction. Japan is developing its own SBAS system, MSAS (MTSAT-based satellite augmentation system; Japanese version of SBAS/WAAS) [5]. MSAS will cover a wide range of latitude (25N to 45N in geographic latitude; 15N to 35N in magnetic latitude) and the lowest magnetic latitude in the coverage is below 15 degrees magnetic north, which is close to the equatorial region.

Ionospheric delay problem is currently the largest concern for MSAS program. Early this year the MSAS Technical Review Board of JCAB (Japan Civil Aviation Bureau) established an Ionosphere Working Group for this problem. Supporting such activities, the authors are investigating the ionospheric effects over Japan to predict and improve the actual performance of MSAS on the ionosphere.

In this paper the authors will describe the performance of the current planar fit algorithm in the low magnetic latitude region with the monitor site configuration for MSAS. The second order quadratic fit will also be tested as well as the first order planar fit. The activities of ionosphere over Japan will be characterized as some system parameters. The height of the actual ionosphere, which the current SBAS assumes as 350 km, is evaluated

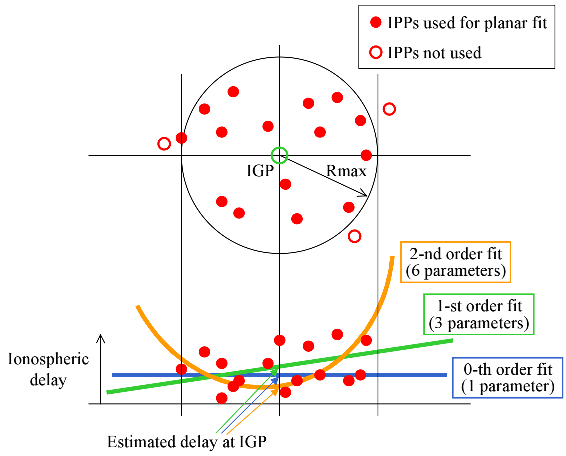

Figure 1. Planar fit algorithm for SBAS ionospheric delay estimation. The current algorithm is the first order planar fit.

through the performance of planar fit. Finally, the performance of storm detector will be characterized and some alternatives are proposed.

SBAS IONOSPHERIC CORRECTION

SBAS ionospheric correction procedure defined in SARPs [1] would be applied to remove ionospheric delay effect and provide precise position to users. SBAS MCS would estimate signal propagation delay at IGPs located every five by five degrees of geographic latitude and longitude within the coverage region, and then broadcast via the SBAS geostationary satellite(s). User receivers apply the broadcast corrections from the IGPs using bi-linear interpolation, in line with SARPs, or MOPS [6] defined for US WAAS.

The broadcast format for propagation delay information (MT18 and MT26) and the correction algorithm in user receivers are well-defined by SARPs while how MCS estimates the propagation delay is open for service providers. Currently it seems that service providers tend to employ conservative procedures and parameters for ionospheric corrections because they must ensure integrity requirements.

The current estimator of ionospheric propagation delay for WAAS and MSAS is known as ‘planar fit’ [7]. For an IGP, the MCS generates a plane which fits the observed vertical ionospheric delays at the surrounding IPPs at the same instant. Then the value at the origin is the delay estimate for the IGP (See Figure 1). Each IPP should be within R_{max} = 2,100 km radius from the IGP. If the number of collected IPPs is less than N_{min} = 10, the planar fit is no longer valid and the IGP is set to ‘not monitored’. Note that the zeroth and second order fit are also drawn in Figure 1 although the current SBAS employs only the first order plane.

The ionospheric delay around the IGP (latitude ϕ_{IGP} and longitude λ_{IGP}) is estimated by

$$\hat{I}_{v,IGP}(\Delta\lambda,\Delta\phi) = \hat{a}_0 + \hat{a}_1 \cdot \Delta\lambda + \hat{a}_2 \cdot \Delta\phi , \tag{1}$$

where $\Delta\lambda = \lambda - \lambda_{IGP}, \Delta\phi = \phi - \phi_{IGP}$. Fitting parameters could be solved by

$$[\hat{a}_0 \quad \hat{a}_1 \quad \hat{a}_2]^{\mathrm{T}} = \left(G \cdot W \cdot G^{\mathrm{T}}\right)^{-1} \cdot G \cdot W \cdot \mathbf{I}_{\mathbf{v,IPP}} , \tag{2}$$

where the observation matrix is

$$G = \begin{bmatrix} 1 & \Delta\lambda_{IPP1} & \Delta\phi_{IPP1} \\ 1 & \Delta\lambda_{IPP2} & \Delta\phi_{IPP2} \\ \vdots & \vdots & \vdots \\ 1 & \Delta\lambda_{IPPn} & \Delta\phi_{IPPn} \end{bmatrix}, \tag{3}$$

and observed vertical ionospheric delay values at IPPs are given by

$$\mathrm{I}_{\mathrm{v,IPP}} = \begin{bmatrix} I_{v,IPP1} \\ I_{v,IPP2} \\ \vdots \\ I_{v,IPPn} \end{bmatrix}. \tag{4}$$

Vertical ionospheric delay at the IGP is equal to $\hat{a}_0$, and Eqn. (1) can be applied at any location around the IGP.

Additionally, the MCS must determine the variance of the estimate as well as the absolute delay, to broadcast GIVE values. User receivers use GIVE (grid ionosphere vertical error) values to compute the confidence bound of position estimate for providing integrity. Once the plane is generated and vertical delay at the origin is estimated, formal error estimate can be computed in terms of 1-sigma expectation.

$$\hat{\sigma}^2_{\hat{I}_{v,IGP}} = \left[\left(G \cdot W \cdot G^{\mathrm{T}}\right)^{-1}\right]_{1,1}. \tag{5}$$

Propagation delays at IPPs are obtained from L1/L2 dual frequency measurements at Monitor Stations with slant-to-vertical conversion below, assuming thin shell ionosphere at the height of H_{iono} = 350 km above the ground,

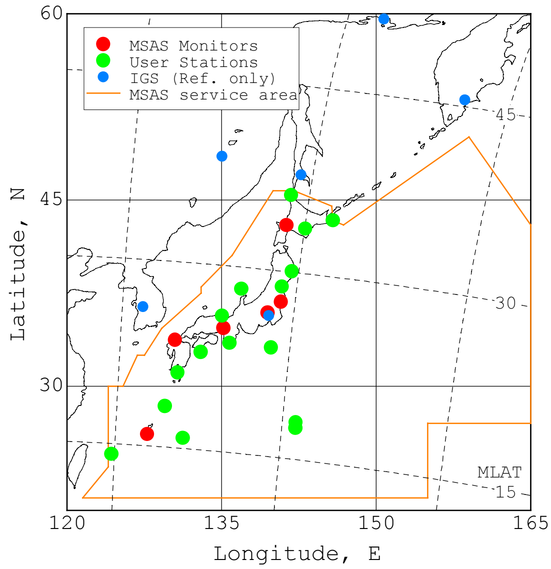

Figure 2. Distribution of observation sites for the dataset.

$$I_v = \sqrt{1 - \left(\frac{R_E}{R_E + H_{iono}} \cos E\right)^2} \cdot I_{slant} , \tag{6}$$

where R_E is radius of the earth; and E is satellite elevation angle above the horizon.

DATASET

For investigating ionospheric effects on SBAS, at first we need appropriate datasets of ionospheric propagation delay observations during quiet and stormy geomagnetic conditions. The datasets should be taken at the monitor stations for the SBAS, but it is not limited to just these, because observations obtained at extra stations are useful for investigating some problems due to sampling density described later.

Ionospheric delay may be measured by different ways: L1/L2 code divergence provides ionospheric delay measurements but are noisy due to multipath on both frequencies; L1 code-carrier divergence has good availability of measurements due to lack of necessity for the relatively weak L2 signal, but is still disturbed by noise; here we have constructed the dataset using L1/L2 carrier divergence which provides very smooth noiseless measurements. Nuisance integer cycle ambiguities involved in carrier phase measurements are removed by averaging to code measurements [8]. Based on temporal continuity of ionospheric delay measurements, cycle slips are detected and removed.

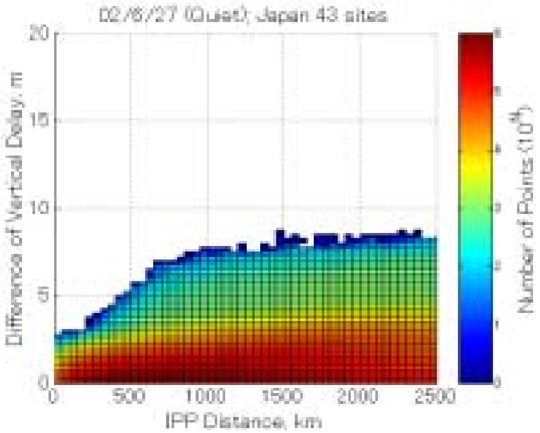

Figure 3. 2-D histogram representing the distribution of differential vertical delays without planar fitting versus IPP separation. No storm detector.

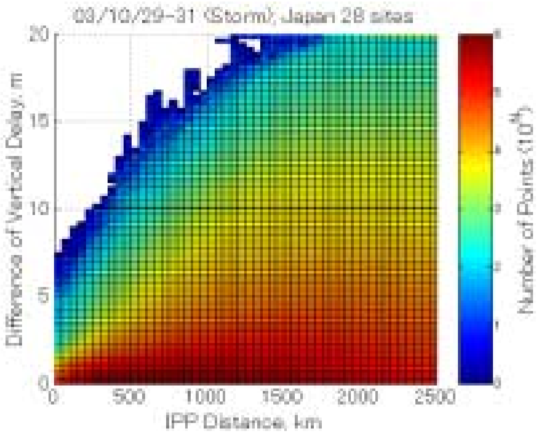

Figure 4. 2-D histogram representing the distribution of differential vertical delays without planar fitting versus IPP separation. This histogram represents stormy condition of ionosphere. No storm detector.

When using dual frequency measurements, an important error source for datasets is instrument bias error between two frequencies inherent to each individual satellite and receiver, sometimes called inter-frequency bias (IFB) [9][10]. A Kalman filter has been applied to estimate such instrument biases [8][11] with an ionospheric model of third-order spherical harmonics basis functions placed on three layers at 250, 350, and 450 km above the ground (a total of 48 unknowns for ionospheric model; plus 27-28 unknowns for satellite IFBs and 28 unknowns for receiver IFBs) in the solar-magnetic coordinates. Elevation mask angle was set to 15 degrees; optimal setting for estimating instrument biases correctly. We confirmed that estimated biases repeated the same values for every analysis even for different periods. Finally, after removing the estimates of instrument biases for each satellite and receiver from the original L1/L2 carrier divergence observation with

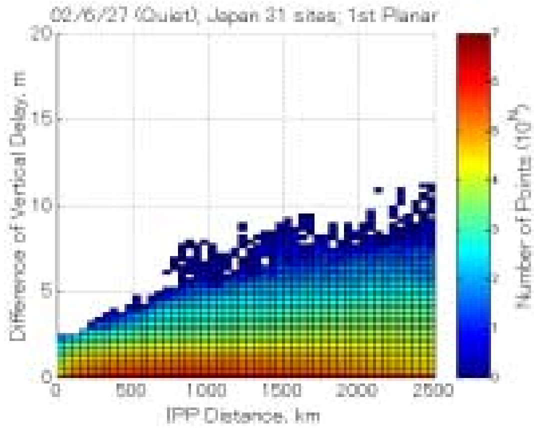

Figure 5. 2-D histogram representing the distribution of differential vertical delays after planar fitting versus IPP separation. No storm detector.

elevation mask at 5 degrees, we have the desired dataset for investigation.

Raw observation data was provided by the GEONET GPS observation network operated by Japan's Geographical Survey Institute since 1994. For these five or more years it has nearly 1,000 stations separated every 20-30 km in Japan, and furthermore it was expanded to have 1,200 stations in this year. All stations in the network have dual-frequency survey-grade GPS receivers and provide their measurements at every 30 seconds in the RINEX format. We chose 28 stations from this network as shown in Figure 2 and created the ionospheric delay datasets without cycle slips or IFBs. 6 IGS stations were also used to improve stability of IFB estimation processes.

Our purpose is surveying how well the SBAS ionospheric correction procedure works in the low magnetic latitude region, in particular around Japan. At first we were interested in the observed uncertainty involved in ionospheric delays. For a typical quiet day, as in Figure 3, the difference of vertical ionospheric delays observed at two IPPs reaches 2-3 meters between zero-distance IPPs, and up to 8 meters between IPPs separated 2,000 km or more. For storm days, Figure 4, it sometimes reaches 7-8 meters for zero-distance, and 15 meters or more even at 1,000 km separation. The problem is now how well the SBAS ionospheric correction procedure could correct such significant uncertainty of ionospheric delays.

CHARACTERIZATION

The ionospheric activity in the low magnetic latitude region, i.e., over Japan, should be characterized for analysis and prediction of the actual system. Some parameters are used for such characterization; σ_{decorr} is

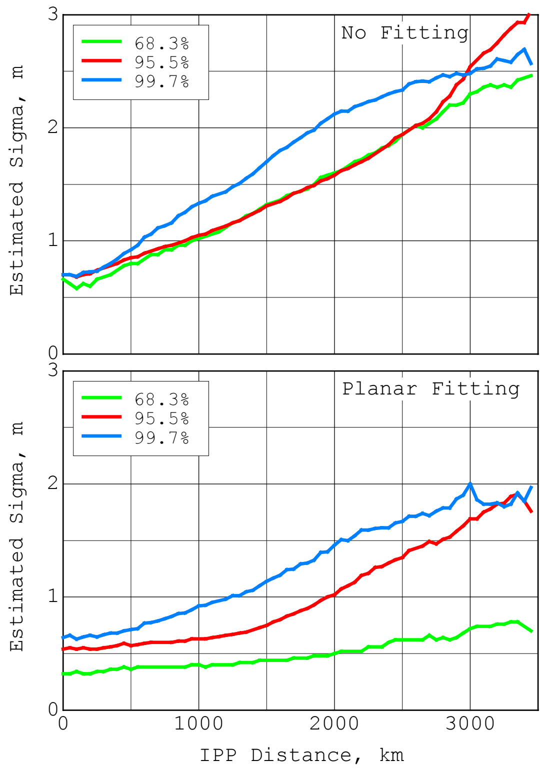

Figure 6. Variance of differential vertical delays, computed based on 1-, 2-, and 3- sigma, versus IPP separation for a quiet ionospheric condition. After planar fit removal, distribution of the residuals becomes away from the normal distribution.

one of them which relates to variance of differential ionospheric delay after removal of a planar fit estimate.

Figure 5 is a 2-dimensional histogram which represents the distribution of differential ionospheric delays after planar fit corresponding to IPP separation for quiet condition of ionosphere (Compare with Figure 3). The differential delays are spatially decorrelated so the distribution becomes compact, but tails of the distribution seems to spread a pretty wide. Note that a total of 31 stations (including all stations in Figure 2) are used to create this plot because characterization of ionosphere should be done with as many stations as possible regardless of the configuration of MSAS monitor stations.

Variance of differential ionospheric delays can be characterized based on 1-, 2-, and 3- sigma values. Figure 6 shows estimated sigma values with and without planar fit removal, versus IPP separation. The bottom plot is with planar fit removal, actually corresponds to the parameter σ_{decorr}. Note that while the distribution of differential ionospheric delays is almost normal without planar fit, after planar fit removal the distribution moves away from the normal distribution with having tails spreading wide. According to 1-sigma plot in the bottom of Figure 6, σ_{decorr} value could be around 35-40 cm, which agrees with the value in CONUS, 35 cm for WAAS [12]. In contrast with case of WAAS, however, three curves in the bottom plot of Figure 6 have clear correlation with IPP separation.

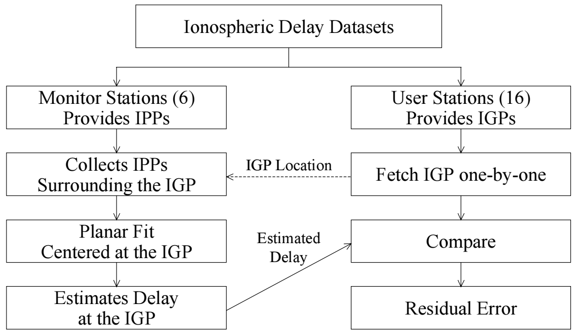

Figure 7. Evaluation Process. Original dataset is divided into two parts. Partial set of Monitor Stations is used for estimating ionospheric delay by planar fit centered at the IGP. Second set of User Stations provides IGP observations to be compared with resulted estimation.

PERFORMANCE OF PLANAR FIT

For evaluating SBAS ionospheric correction capability, we applied the planar fit algorithm to the observed ionospheric delay datasets described above. At first, the original dataset is divided into two parts; sets of Monitor Stations and User Stations (Figure 7).

MSAS has 6 monitor stations in Japan, so we applied planar fit algorithm based on IPPs collected by 6 GEONET stations co-located by MSAS monitor stations (Red stations in Figure 2). These stations should be called as Monitor Stations which provide IPP measurements to be used for analysis.

In order to evaluate the performance of the algorithms at the IGP, we have used 16 stations (Green stations in Figure 2) other than MSAS 6 monitor stations. Because SBAS must bound user positioning error at any (unknown) user location, we need to evaluate its performance using these User Stations which provide IGP measurements, other than Monitor Stations above.

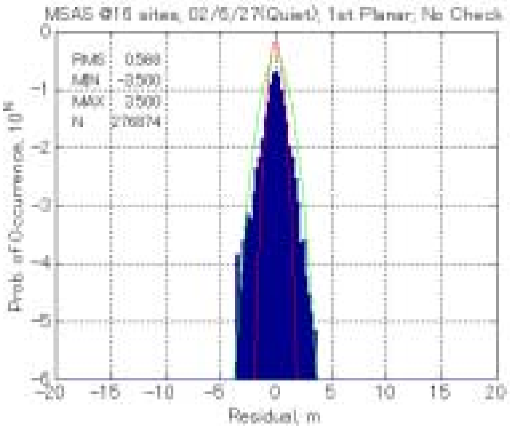

Figure 8. Histogram plots of planar fit residuals for quiet condition.

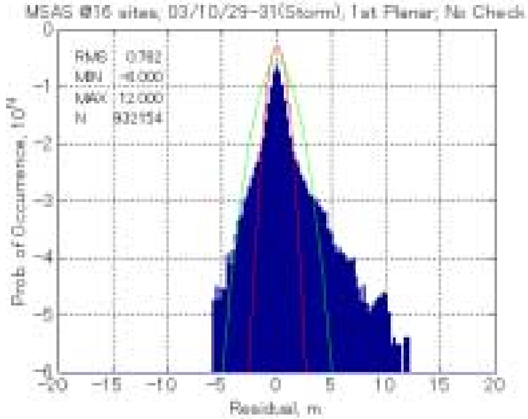

Figure 10. Histogram plots of planar fit residuals for storm condition. Compare with Figure 5.

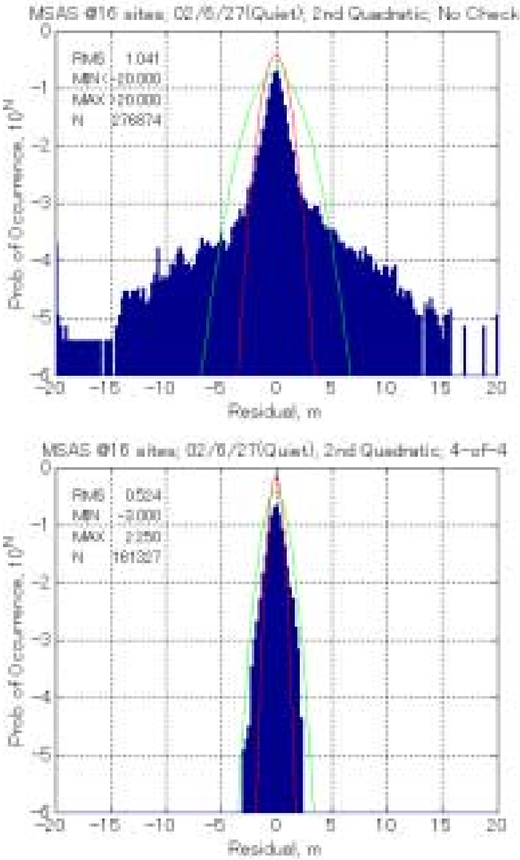

Figure 9. (Top) Histogram plots of quadratic fit (second order) residuals for quiet condition. (Bottom) Applied 4-of-4 geometry check and removed IGPs with bad geometry. IGP availability decreased to 58.3%.

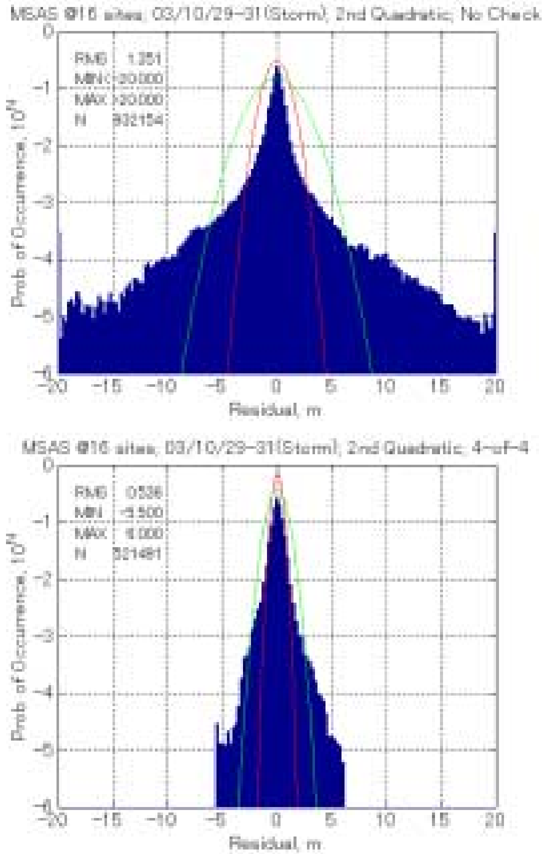

Figure 11. (Top) Histogram plots of quadratic fit (second order) residuals for storm condition. (Bottom) Applied 4-of-4 geometry check and removed IGPs with bad geometry. IGP availability decreased to 55.9%.

In this analysis, each residual error was obtained as the difference between IGP vertical delay observed from User Stations and the corresponding vertical delay estimation computed by IPPs surrounding the IGP observed from Monitor Stations. Vertical delays observed from Monitor Stations have not been used as IGPs.

Planar and Quadratic Fit: Quiet and Storm

Figure 8 shows a histogram plot of residual errors after planar fit removal for quiet ionospheric condition. RMS residual was 0.564 meter and residual errors were bounded within 3.56 meters although no storm detectors applied.

One possible way to improve correction performance may be applying quadratic fit (second order fitting). Vertical ionospheric delay should be modeled below instead of Eqn. (1),

$$\hat{I}_{v,IGP}(\Delta\lambda,\Delta\phi) = \hat{a}_0 + \hat{a}_1 \cdot \Delta\lambda + \hat{a}_2 \cdot \Delta\phi + \hat{a}_3 \cdot \Delta\lambda \cdot \Delta\phi + \hat{a}_4 \cdot (\Delta\lambda)^2 + \hat{a}_5 \cdot (\Delta\phi)^2, \quad (7)$$

where 6 fitting parameters can be solved by the similar way to Eqn. (2).

Figure 9 gives the sample results of quadratic fit for quiet ionospheric condition. Unfortunately RMS residual was 1.043 meters so not improved against planar fit , and more importantly, large correction errors sometimes occur. This is because increasing the number of fit parameters causes a reduction of the number of degrees-of-freedom and the geometries of the IPP distribution was not good enough to perform a quadratic fit.

To confirm this, Figure 9 (b) shows quadratic fit results only for IGPs which have good geometry. A 4-of-4 check was applied here; the IGP must have at least one IPP in each of its 4 quadrants. With this geometry checking, RMS residual was 0.520 meters and the maximum residual was improved to 2.94 meters. But the number of evaluated IGPs was 58.3% of the case without geometry check; this 4-of-4 geometry check lowered the availability of IGP. The quadratic fit essentially has better correction capability, but it would provide relatively low number of available IGPs.

Now we are going on to the storm condition. The planar fit is applied to the dataset taken during storm ionospheric conditions, represented in Figure 4. The histogram plot of resulting residual error is illustrated in Figure 10. RMS residual error grew 0.759 meter and the maximum was 12.02 meters. The asymmetric histogram involves many positive large residuals; this means there are large 'mountains' to which planar fit cannot correct properly.

A quadratic fit has the capability to correct such large 'mountains' according to Figure 11 (b) which has the property of symmetry. However, the quadratic fit still requires some geometry check. The performances of planar and quadratic fit are summarized in Table 1.

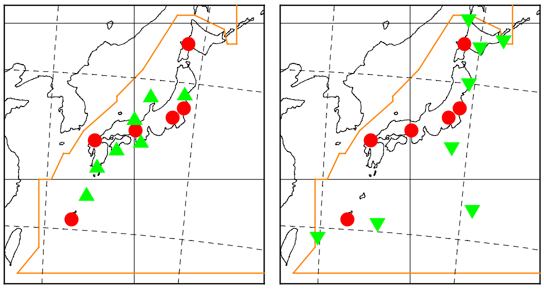

Figure 12. The distribution of User Stations for consideration of geometry of monitor stations; (Left) User Stations inside the network of Monitor Stations; (Right) User Stations outside the network. Red circles represent the network of MSAS Monitor Stations.

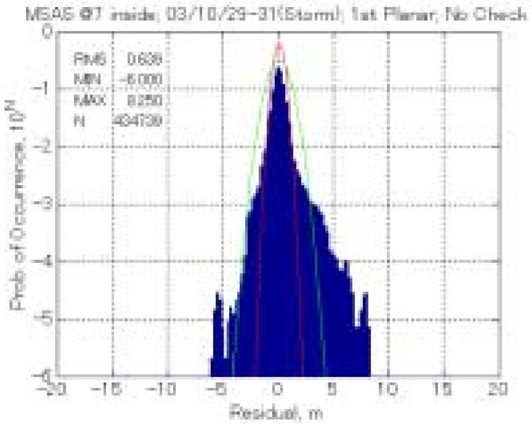

(a) Inside stations

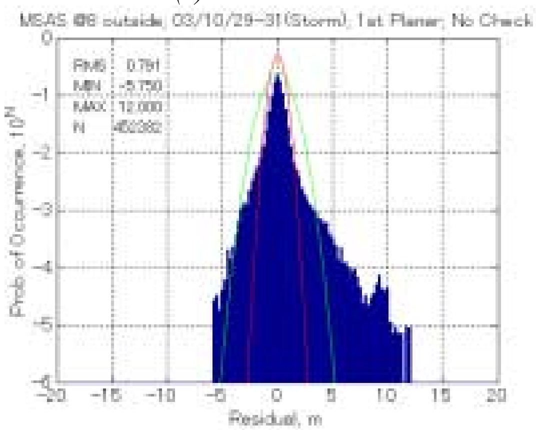

(b) Outside stations

Figure 13. Histogram plots of planar fit residuals for storm condition. (a) User stations are located inside the network of Monitor Stations; (b) User stations are outside the network.

Geometry of Monitor Stations

The residual errors of ionospheric correction caused by the SBAS procedure can be decomposed as: (i) measure-

Table 1. Performance of Planar Fit

Condition	User Station Set	Order	Geometry Check	Residuals, m		Evaluated IPPs
				RMS	Max.	
Quiet	Whole 16	1	No	0.564	3.56	67.6 %
		2	No	1.04	22.5	
		1	4-of-4	0.498	2.91	39.4 %
		2	4-of-4	0.520	2.94	
Storm	Whole 16	1	No	0.759	12.0	68.1 %
		2	No	1.58	92.8	
		1	4-of-4	0.551	5.68	38.1 %
		2	4-of-4	0.531	5.94	
	Inside 7	1	No	0.635	8.30	53.1 %
		2	No	0.620	24.8	
		1	4-of-4	0.525	5.68	37.7 %
		2	4-of-4	0.479	5.52	
	Outside 8	1	No	0.787	12.0	52.0 %
		2	No	1.67	77.9	
		1	4-of-4	0.5678	7.65	23.4 %
		2	4-of-4	0.5683	8.70	

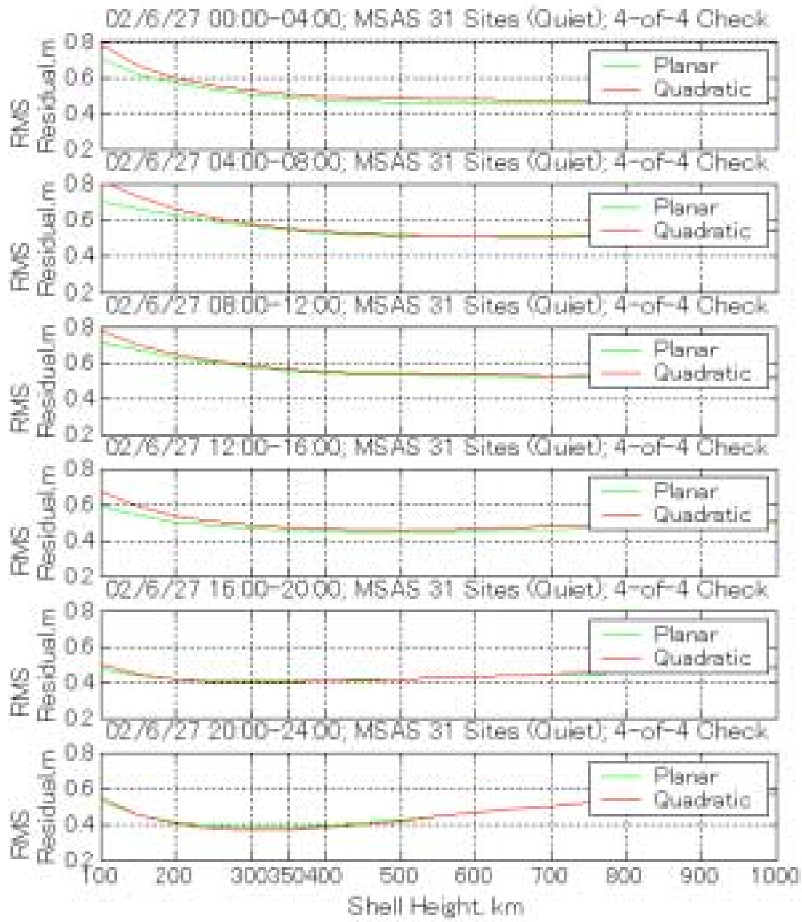

Figure 14. The performance of planar fit with respect to shell height. Local time is UT+9h.

ment error at the monitor stations (cycle slips, multipath, etc.); (ii) undersampling (MSAS has only 6 monitor stations); (iii) thin shell assumption; (iv) ionospheric height assumption (350 km for SBAS); (v) spatial resolution of correction information (five by five degrees); (vi) broadcasting interval (maximum 5 minutes); (vii) quantization error (0.125 meter in MT26). We evaluated effects of (ii), (iii), and (iv) in Figures 8-11. Here the effect of (ii) undersampling problem has an emphasis.

Again, Figure 13 relates to the performance of the first order planar fit for storm condition of ionosphere. Histogram plot (a) shows resulted residual errors after planar fit at IGPs observed from 7 of 16 User Stations located inside the network of Monitor Stations. (b) displays evaluation by the other 8 User Stations located outside the network. Both results are without any geometry check nor storm detectors. The distribution of User Stations is illustrated in Figure 12.

The first order planar fit for inside stations resulted in RMS residuals of 0.635 meter while 0.787 meter for outside stations. The maximum residuals were 8.30 meters and 12.04 meters, respectively. Comparing Figure 13 (b) with Figure 10, these Figures are almost identical, we can see that most of large residual errors are corresponding to outside stations.

While the RMS of residual errors are almost identical for both sets of stations, the largest error were 5.68 meters for inside stations and 7.65 meters for outside stations.

Shell Height Consideration

For the current SBAS, the ionosphere is assumed to be at a thin shell with the fixed height of 350 km. It is well known the actual ionosphere is not stationary and changes the height due to time of the day as well as season in the year and solar activities.

Figure 14 demonstrates the relationship between shell height assumption and the fitting performance. RMS residual error is the lowest when the shell height is set to 500 km or more during daytime (00-12h UT; 09-21h local). At local night, the height of ionosphere which provides the best performance decreased, and in the early morning (20-24h UT; 05-09 local) it was at 350 km.

The difference in RMS for various shell height is, however, only 0.1 meter or less. In comparison with the complexity of mechanism for changing shell height in the MCS and/or user receivers, this potential improvement of the ionospheric model is relatively small.

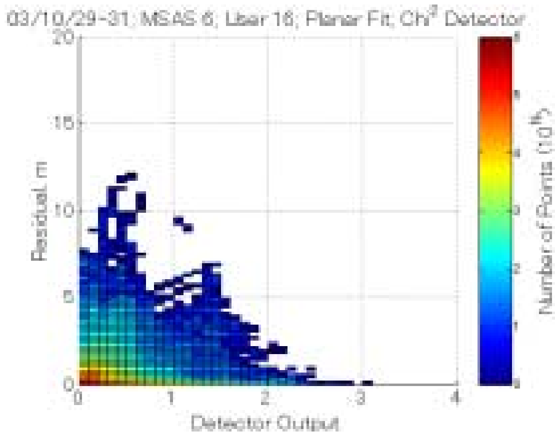

Figure 15. Performance of chi-square storm detector. Each IPP is determined as storm condition if the corresponding monitor output is greater than 1.

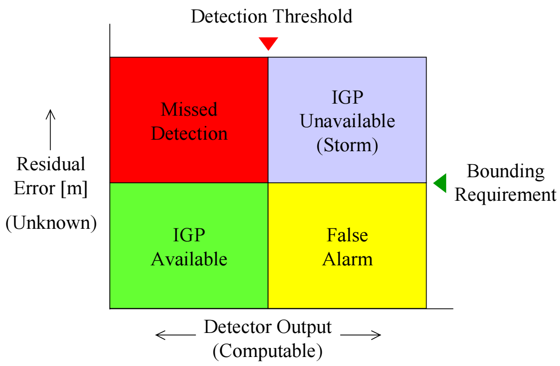

Figure 16. Definition of IGP status. Note that residual error is unknown for the actual system.

STORM DETECTOR

In case of MSAS, one reason for relatively low availability for APV operations is that most IGPs will be set as being in the storm condition for which users could not expect valid ionospheric correction, even for nominal condition. It seemed that the chi-square storm detector currently built in MSAS MCS algorithm has worked in very sensitive or conservative manner.

This fact motivated us to consider of detection algorithms other than one based on chi-square test. If there is an algorithm to detect storm condition of ionosphere better than chi-square test, it could improve the availability for APV operations. First of all, chi-square statistics for storm condition are shown in Figure 15. Ideally, residual errors should be small if the detector output is less than 1; on the other hand, the detector must indicate storm condition with the corresponding output greater than 1 in case of large residual error. The current chi-square detector, unfortunately, implies no such feature.

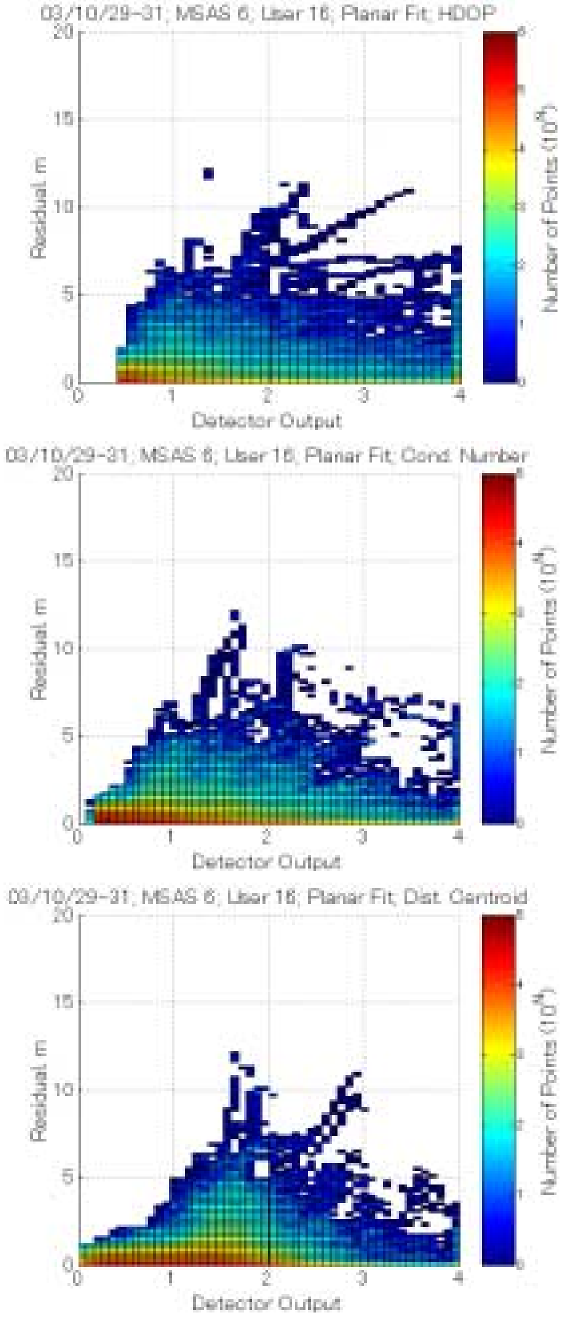

Figure 17. The performance plots for three candidate storm detector algorithms during October 2003 storm. Compare with Figure 15 for the current chi-square detector.

In our analysis, each candidate storm detector works based on the IPPs observed from 6 MSAS Monitor Stations. The output of detector is indicated as horizontal axis. The residual errors are computed for IGPs observed from the other 16 User Stations, as same to case of Figures 7-11, and relate to the vertical axis of the following 2-D histogram plots.

Figure 16 defines some status of IGP. Each IGP is determined as available if the corresponding detector output is less than a certain threshold; in this case, missed detection would occur if actual residual error exceeds the bounding requirement. When detector output is greater than the threshold, the IGP is declared unavailable; if the actual residual error is less than the requirement, this is a false alarm condition. Note that missed detection and false alarm conditions cannot be recognized for the actual system because the residual error at user location is unknown.

We have tested three candidate algorithms for a storm detector:

1. HDOP: computed based on geometry matrix relative to the IGP location (height could be set to zero) with IPPs used for planar fit.
2. Condition Number: of the matrix used for planar fit.
3. Distance to Centroid: The distance between IGP and the centroid of IPPs used for planar fit.

IPPs could be weighted based on the corresponding satellite elevation angle.

The performances of the candidate algorithms are evaluated with dataset during October 2003 storm. Figure 17 shows the relationship between residual errors and detector outputs. In comparison with Figure 14, these three algorithms give better performance but false alarm could not be lowered sufficiently.

Given bounding requirement and missed detection rate, one can determine the detection threshold and therefore compute resulted false alarm rate. Table 2 summarizes the performances of the candidate detectors in terms of false alarm rate with bounding requirement of 5 meters. The current chi-square detector could give low false alarm rate but resulted a lot of missed detection. For missed detection rate 0.001, each algorithm reduces false alarm rate down to 40% while chi-square detector resulted false alarm of 90%.

Note that the results shown here actually involve undersampling effects. These candidate detectors measure

Table 2. The performances of the candidate detectors (Bounding Req. = 5 m).

Algorithm	Missed Detection Rate	Detection Threshold	False Alarm Rate
Chi-square	0.897	1.000	0.0149
	0.001	0.0352	0.920
HDOP	0.001	0.793	0.401
Cond. number	0.001	0.783	0.406
Dist. to centroid	0.001	1.153	0.463

goodness (or badness) of 'geometry' of IPPs for planar fit distributed around the IGP. If there is a large hole in the distribution of IPP, i.e., there is a large area not sampled by the monitor stations, these detectors would determine the IGP is in 'storm condition'. Such conditions do not always relate to the actual storm in fact, but the corresponding residual error can be expected to be large. This is a reason we evaluated detectors at 16 User Stations other than MSAS Monitor Stations.

Note also that the operational systems of WAAS and MSAS have a certain mechanism to involve such geometric metrics, as undersampled threat model, additional to the chi-square storm detector. Although the chi-square detector passes over a lot of missed detection conditions, the model will bound the actual user ranging error.

CONCLUDING REMARKS

The authors evaluated the current SBAS ionospheric correction capability over Japan. The planar fit algorithm fortunately gave relatively satisfactory performance in such low magnetic latitude region for LNAV/VNAV operations. The algorithm for storm detector might be modified so reducing false alarm rate for achieving the capability of APV operations. We also evaluated undersampling effects by using additional pseudo-user stations which is essential for ensuring integrity of SBAS.

Further investigations should include: evaluating other correction methods such as multi-layer ionospheric model or Kriging algorithm; sorting out the relationship between storm detector and undersampling (essentially geometry) problem; considering temporal variations of ionosphere; and studying scintillation effects.

ENRI is currently constructing an observation station in Ishigaki Island (Southwest edge of Japan, 15N magnetic) for investigating scintillation effects. This would be useful for analysis of temporal variations of ionosphere as well as scintillation.

REFERENCES

[1] *International Standards and Recommended Practices, Aeronautical Telecommunications*, Annex 10 to the Convention on International Civil Aviation, vol. I, ICAO, Nov. 2002.

[2] A. Komjathy, L. Sparks, A. Mannucci, and X. Pi, An Assessment of the Current WAAS Ionospheric Correction Algorithm in the South American Region, *Navigation*, vol. 50, no. 3, pp. 193-204, Fall 2003.

[3] P. Doherty, S. Delay, C. Valladares, and J. Klobuchar, Ionospheric Scintillation Effects on GPS in the Equatorial and Auroral Regions, *Navigation*, vol. 50, no. 4, pp. 235-245, Winter 2003-2004.

[4] K. Matsunaga, K. Hoshinoo, and K. Igarashi, Observations of Ionospheric Scintillation on GPS Signals in Japan, *Navigation*, vol. 50, no. 1, pp. 1-7, Spring 2003.

[5] J. Imamura, MSAS Program and Overview, *Proc. 4th CGSIC IISC Asia Pacific Rim Meeting*, 2003 Joint International Conference on GPS/GNSS, Tokyo, Nov. 2003.

[6] *Minimum Operational Performance Standards for Global Positioning System/Wide Area Augmentation System Airborne Equipment*, DO-229C, RTCA, Nov. 2001.

[7] T. Walter, A. Hansen, J. Blanch, and P. Enge, Robust Detection of Ionospheric Irregularities, *Proc. ION GPS*, pp. 209-218, Salt Lake City, UT, Sept. 2000.

[8] A. Hansen, *Tomographic Estimation of the Ionosphere Using Terrestrial GPS Sensors*, Ph.D. Dissertation, Stanford University, March 2002.

[9] David S. Coco, Clayton Coker, Scott R. Dahlke, and James R. Clynch, Variability of GPS satellite differential group delay biases, *IEEE Trans. Aerospace and Electronic Systems*, vol. 27, no. 6, pp. 931-938, Nov. 1991.

[10] Brian D. Wilson, Colleen H. Yinger, William A. Feess, and Chris Shank, New and Improved: The Broadcast Interfrequency Biases, *GPS World*, pp. 56-66, Sept. 1999.

[11] A. J. Mannucci, B. D. Wilson, D. N. Yuan, C. H. Ho, U. J. Lindqwister, and T. F. Runge, A global mapping technique for GPS-derived ionospheric total electron content measurements, *Radio Science*, vol. 33, no. 3, pp. 565-582, May-June 1998.

[12] A. Hansen, J. Blanch, T. Walter, and P. Enge, Ionospheric Correlation Analysis for WAAS: Quiet and Stormy, *Proc. ION GPS*, pp. 634-642, Salt Lake City, UT, Sept. 2000.